

Properties of the Silica Layer during the Formation of MCM-41 Studied by EPR of a Silica-Bound Spin Probe

Debbie Baute,[†] Veronica Frydman,[‡] Herbert Zimmermann,[§] Shifi Kababya,[†] and Daniella Goldfarb^{*,†}

Department of Chemical Physics and Chemical Research Support Unit, Weizmann Institute of Science, Rehovot, Israel, and Max-Planck Institute for Medical Research, Heidelberg, Germany

Received: December 1, 2004; In Final Form: February 25, 2005

The properties of the silica layer during the formation of the mesoporous material MCM-41 were investigated by electron paramagnetic resonance (EPR) experiments carried out on a specifically designed, organo(trialkoxo)silane spin probe, SL1SiEt. Minute amounts of the spin probe were co-condensed with the silica source, tetraethyl orthosilicate (TEOS), in the synthesis of MCM-41 with cetyltrimethylammonium bromide (CTAB) under basic conditions. The mobility and location of the spin probe were followed in the CTAB micellar solution before the reaction, in the reaction mixture and in the final ordered material. It was found that the EPR spectra of hydrolyzed SL1SiEt throughout the room temperature part of the reaction are characteristic of a fast tumbling species, indicating that the silica is highly fluid prior to drying. After filtering, a slow motion type spectrum was observed, showing that the spin-label experiences considerable motional hindrance. The liquidlike behavior could be restored upon stirring the material in water. When the reaction is performed with a hydrothermal stage, the spectrum of SL1SiEt in the final product is the same as that of the room temperature synthesized material, but the addition of water did not restore the high mobility, due to a higher degree of silica cross-linking. The location of SL1SiEt throughout the formation process was obtained from electron spin-echo envelope modulation (ESEEM) measurements on MCM-41 prepared with CTAB deuterated either at the *N*-methyl or the α position and in a reaction carried out in D₂O. Comparing the deuterium modulation depth, $k(^2\text{H})$, induced by CTAB- α -*d*₂, CTAB-*d*₉, or D₂O in CTAB micellar solutions of a number of reference spin probes with those of SL1SiEt revealed that the hydrolyzed SL1SiEt is located near the polar heads of the surfactant in the absence of base and TEOS. This supports the postulation of charge matching at the interface as a driving force for the formation of the mesostructure. Similar experiments carried out on reaction mixtures containing SL1SiEt showed a decrease of $k(^2\text{H})$ from CTAB- α -*d*₂ and CTAB-*d*₉ compared to the micellar solution, exhibiting practically no time dependence. This indicates that the spin probe is pulled away from the micelle-water interface into the loosely linked, forming silica network. After drying, the modulation depth induced by CTAB- α -*d*₂ and CTAB-*d*₉ increases, showing that, once the water is removed, the silica walls contract around the micelles, pushing the silica-linked spin probe into the organic phase within the mesopores.

Introduction

Numerous studies on templated mesoporous materials have emerged in the past decade, sparked by the discovery of the M41S family in 1992.^{1,2} Since then, these materials have been the subject of extensive investigations on potential applications in fields ranging from separation and catalysis to electronics.^{3–5} The three members of the M41S family are the hexagonal MCM-41, the lamellar MCM-50 and the cubic MCM-48. By far, the most attention has been devoted to MCM-41 because of its straightforward synthesis and thermal stability.^{3,4,6} In general, templated mesoporous materials form through the polymerization of silica precursors around assemblies of surfactant molecules. Hence, a whole variety of materials can be prepared with different pore topologies and overall properties,

using different templates and/or inorganic precursors and varying the reaction conditions.^{4,6}

Understanding the interaction between the surfactant and the inorganic precursor is vital to unraveling the details of the formation mechanism of templated mesoporous materials. Surfactant molecules in aqueous solution arrange themselves into different structures (spherical/rod-shaped micelles or hexagonal/cubic/lamellar liquid crystal (LC) phases), according to their concentration, structure, pH, temperature, ionic strength and so on.⁷ Different models describing the interaction of the inorganic phase with the surfactant molecules have been suggested and reviewed.^{6,8} The first two mechanisms were proposed by the Mobil group.^{1,2} In the first, the inorganic precursor forms an amorphous solid around the polar head region of a preformed liquid crystal phase of surfactant molecules.⁹ In the second, which applies to solutions of low surfactant concentrations—above the critical micelle concentration but well below the concentration required to form a liquid crystal phase—the addition of the silica source induces the formation of the long-range order.¹⁰ In another model, the

* Author for correspondence. E-mail: daniella.goldfarb@weizmann.ac.il. Telephone: +972-8-9342016. Fax: +972-8-9344123.

[†] Department of Chemical Physics, Weizmann Institute of Science.

[‡] Chemical Research Support Unit, Weizmann Institute of Science.

[§] Max-Planck Institute for Medical Research.

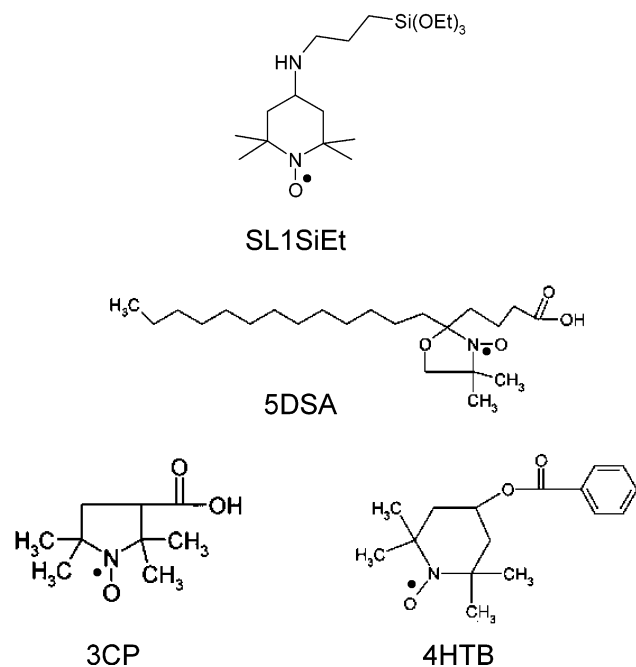


Figure 1. Spin-label SL1SiEt and the reference spin probes used in this study in decreasing order of hydrophilicity: 3-carboxyproxyl (3CP), 5-doxyl stearic acid (5DSA), and 4-hydroxy-TEMPO-benzoate (4HTB).

silicate oligomers do not adsorb on the micellar interface but instead form siliceous prepolymers that bind free surfactants, where the micelles serve only as a reservoir for the surfactant molecules.¹¹

A cooperative self-assembly process based on electrostatic interactions between the charged surfactants and the inorganic components is now considered to trigger the formation of the long-range order.¹² There are several possible routes of which the basic one (S^+I^-), usually involving an alkylammonium surfactant (S^+) and anionic silica species (I^-) easily obtained under basic conditions, leads to the M41S-type materials.¹³ It was shown using 2H NMR that under conditions where the silicate polymerization is suppressed, a silicatropic liquid crystalline mesophase can form upon mixing a micellar solution of charged surfactants and sodium silicate in the presence of methanol.^{14,15} Nevertheless, more detailed information on the formation mechanism for individual reaction processes is needed for understanding and tailoring the properties of these silica-based solids. In situ studies of the MCM-41 formation give information on the progress of the reaction as a function of time. Such studies have been performed with NMR,¹⁶ FTIR,¹⁷ and XRD.^{18,19} Another efficient and established method is EPR of spin probes, which provides insight into the polarity of the spin-labels' microenvironment and their motional characteristics and thereby reflects on the system itself. This method has been applied to the reaction mixtures of MCM-41^{20–23} and SBA-15.^{24,25} In all these studies the spin-probes selected were surfactant-like and therefore they probed primarily events in the organic phase, while providing indirect information on the formation and properties of the silica layer. Nitroxide spin probes have also been used to monitor structural and chemical changes occurring during silica sol–gel–xerogel transitions. In this particular case 4-oxo-TEMPO was used and gradual changes in line widths, rotational correlation time, isotropic hyperfine interaction parameters and integral line intensities were observed.²⁶

In the present work, a specifically designed, siloxane-based spin-label, SL1SiEt (shown in Figure 1), was used in situ

investigations of the synthesis of MCM-41 to explore the properties of the forming silica layer and its interaction with the template molecules. The design of the probe was based on recent efforts toward functionalizing mesoporous materials, to expand the range of reactive species that can be used in catalysis and to change the properties of the silica surface.^{27–34} Of specific interest to this study are the attempts made to incorporate organo(trialkoxo)silanes in the silica matrix. Initially, postsynthesis grafting of organo(trialkoxo)silanes onto preformed MCM-41 was the preferred method, but it suffers from certain disadvantages of which the most important ones are the lack of control over loading and the possibility of obtaining a variety of surface bound species.³³ Consequently, ways were sought and found to introduce organic moieties into the silica wall, creating the so-called hybrid organic–inorganic materials.^{27–34} These were based on functionalized silicagels, known as polysilsesquioxanes, which had already been prepared with an extensive variety of organo(trialkoxo)silane monomer precursors.^{30,31} Ordered organomodified silicas have been prepared, in which the silica source was either a double trialkoxysilyl precursor²⁹ or a mixture of tetraethyl orthosilicate (TEOS) and an organosilane.^{34,35} In particular, the work of Mann et al. demonstrates the feasibility of co-condensation to incorporate various organic groups into mesoporous materials following the S^+I^- pathway, used to obtain MCM-41.³⁶ A noteworthy example is the incorporation of 3-(aminopropyl)triethoxysilane (ATES) into the silica network by template-directed co-condensation.²⁸ There, ^{29}Si MAS NMR spectroscopy of the as-synthesized materials showed that the distribution of the organic moieties was homogeneous throughout the inorganic network.

In the present study, we used a nitroxide TEMPO radical attached to such an ATES chain (see Figure 1). A similar sol–gel entrapped TEMPO has previously been used as a catalyst for the selective oxidation of methyl- α -D-glucopyranoside.³⁷ Unlike earlier work where the radical was covalently linked to a functionalized aminopropyl silica, this study employed copolycondensation of the radical precursor with tetramethyl orthosilicate (TMOS), leading to a material with higher catalytic performance.³⁷ No leaching of the radical took place and its EPR spectrum did not undergo changes upon consecutive runs. In a recent work, the spin-labeled silica precursor, doxyl-TMOS (*N*-propyltrimethoxysilane-5-doxylstearamide), was used to study mesoporous silica formed via the neutral templating route using dodecylamine.³⁸ In this case, the spin-label is situated nine bonds away from the silane group (compared to five in our case), which makes it more sensitive to the events occurring in the organic phase than to those in the silica layer.

When the spin-label is incorporated in the material, it should feel changes in its motional characteristics caused by the progress in the polymerization of the silica. These changes are expected to be reflected in the line shape of the EPR spectrum. Moreover, variations in the local polarity should be manifested in the ^{14}N hyperfine coupling.³⁹ The location of the spin-label within the forming mesostructure and its interaction with the surfactant molecules can be determined by electron spin–echo envelope modulation (ESEEM) experiments. This technique allows to determine weak anisotropic hyperfine interactions with nearby nuclear spins. These are expressed as modulations in the electron spin echo decay, and the observed modulation depth, k , is a measure of the electron–nuclear distance, the number of neighboring nuclei and the nuclear spin.⁴⁰ The three pulse echo intensity for an electron spin $S = 1/2$ interacting with a single nucleus, $I = 1$, is⁴¹

$$V(T) = \frac{1}{2}[V_{\alpha}(T) + V_{\beta}(T)]$$

$$V_{\alpha}(T) = 1 - \frac{16}{3}K \sin^2\left(\frac{\omega_{\beta}\tau}{2}\right) \sin^2\left(\frac{\omega_{\beta}(\tau + T)}{2}\right) + \frac{16}{3}K^2 \sin^4\left(\frac{\omega_{\alpha}\tau}{2}\right) \sin^4\left(\frac{\omega_{\beta}(\tau + T)}{2}\right)$$

$$V_{\beta}(T) = 1 - \frac{16}{3}K \sin^2\left(\frac{\omega_{\alpha}(\tau + T)}{2}\right) \sin^2\left(\frac{\omega_{\beta}\tau}{2}\right) + \frac{16}{3}K^2 \sin^4\left(\frac{\omega_{\alpha}(\tau + T)}{2}\right) \sin^4\left(\frac{\omega_{\beta}\tau}{2}\right)$$

K is the modulation depth parameter given by $K = (\omega_n B / \omega_{\alpha} \omega_{\beta})$ where $\omega_n = \gamma_n H_0 / \hbar$ is the nuclear Larmor frequency and H_0 is the magnetic field, T and τ are time intervals (see Figure 2a), ω_{α} and ω_{β} are the so-called ENDOR frequencies given by

$$\omega_{\alpha} = \left[\left(\frac{A}{2} + \omega_n \right)^2 + \left(\frac{B}{2} \right)^2 \right]^{1/2}, \quad \omega_{\beta} = \left[\left(\frac{A}{2} - \omega_n \right)^2 + \left(\frac{B}{2} \right)^2 \right]^{1/2}$$

When the point-dipole approximation applies $A = \gamma_e \gamma_n \hbar r^3 (3 \cos^2 \theta - 1)$, $B = \gamma_e \gamma_n \hbar r^3 (3 \cos \theta \sin \theta)$, r is the electron–nuclear distance, and θ is the angle between \vec{r} and the magnetic field direction. Hence, the shorter the distance the larger is K . In the above, the relaxation and the nuclear quadrupole interaction have been neglected. The above equations hold for a single electron–nuclear pair with a particular r and θ . In the case of frozen solutions or systems with a certain degree of disorder, the ESEEM trace is a superposition of individual traces, each corresponding to a single r and θ pair. For a weak hyperfine interaction, $\omega_{\alpha} \sim \omega_{\beta} \sim \omega_n$, this yields a modulation frequency of ω_n and some effective modulation depth, k , as shown in Figure 2b.

When the electron spin interacts with several nuclei, the echo intensity is⁴¹

$$V(T) = \frac{1}{2} \left[\prod_{i=1}^n V_{\alpha i}(T) + \prod_{i=1}^n V_{\beta i}(T) \right]$$

which leads to a further increase in the effective modulation depth.

This method has been applied previously in the investigation of the micellar environment of surfactant-like spin probes during the formation of MCM-41^{21,22} and SBA-15.^{24,25} The relative location of the spin probes was obtained from the deuterium modulation depth, $k(^2\text{H})$, of reaction gels in D_2O or with specifically labeled ^2H surfactant molecules. In the present work, ESEEM is implemented to determine the environment of a silica-bound spin-label, SL1SiEt. The focus is again on $k(^2\text{H})$, reflecting the interaction between the unpaired electron of SL1SiEt and the deuterium nuclei located at different places along the chain of the cetyltrimethylammonium bromide (CTAB) surfactant, or in the surrounding water. Applying this method to a set of reference spin-labels of which the location can be anticipated, based on their hydrophilicity and previous studies, enabled us to draw up a model of the environment of SL1SiEt and the silica layer properties at different stages of the reaction.

Experimental Section

Synthesis of Surfactant and Spin-Label. The 2,2,6,6-tetramethyl-4-[3-(triethoxysilyl)propylamino]-1-piperidinoxy spin-label, SL1SiEt (Figure 1), was synthesized following a

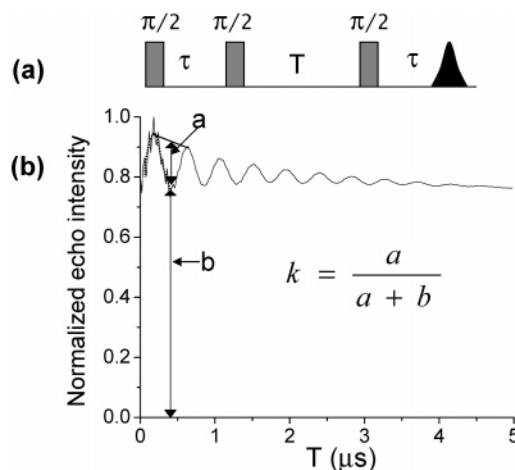


Figure 2. (a) Three pulse ESEEM sequence. (b) Example of a three pulse ESEEM trace of RT-MCM-41 (SL1SiEt) prepared with CTAB- d_9 , recorded at 3456 G, $\tau = 204$ ns, with indication of $k(^2\text{H})$.

procedure analogous to the one described in the literature for the preparation of the trimethoxysilyl derivative, using a organo-(triethoxy)silane instead of a methoxysilane.³⁷ The spin-label was not extracted from its reaction mixture, since the aqueous workup that is usually applied in similar reactions, caused the spin-label to polymerize. Hence, the whole solution (0.51 M in MeOH) was used as such. Since only minute amounts were used, the presence of the MeOH did not affect the reaction.

The *N*-methyl deuterated cetyltrimethylammonium- d_9 bromide (CTAB- d_9) surfactant was prepared according to the literature.^{42,43} A 5 g sample of *n*-hexadecylamine (0.016 mol, Aldrich) was dissolved in 200 mL of methanol containing 6.4 g of NaOH, after which the mixture was cooled to 0° C and 91.2 g of CD_3I (40 mL, Aldrich, 0.63 mol) was added. The mixture was stirred overnight in an ice-cooled, tightly closed reaction flask and was then left for 4 days at room temperature. The solution was evaporated to dryness, triturated with 150 mL chloroform, filtered from the sodium iodide and evaporated under reduced pressure. A chromatography column filled with 500 g of the anion-exchange-resin AGR I-X4 (100–200 mesh, Biorad) in the chloride-form was transformed into the bromide-form with an aqueous solution of 5% sodium bromide. The column was washed with water until the bromide could not be detected anymore. The water was gradually replaced by methanol and the resin was kept for 2 days under this condition. The cetyltrimethylammonium- d_9 -iodide was transformed to the corresponding bromide using this resin and the final product was further purified by recrystallization. The chemical and isotopic purity of the compound was checked by ^1H NMR (250 MHz, CDCl_3/TMS) and found to be better than 99%. CTAB- d_2 was prepared according to the literature.^{14,44}

Synthesis of MCM-41. Two different methods were used to prepare MCM-41. In the first one, NaOH was the base catalyst, following the procedure of Fowler et al.,²⁸ while in the other NH_4OH was employed. Small amounts were used, due to the enriched materials. In a typical synthesis of the first kind 0.1 g of CTAB (BDH Laboratory Supplies) was dissolved in 4.4 mL of doubly distilled H_2O . After a few minutes of stirring, 1.25 mL of NaOH 1 M (Merck) was added, followed by 0.46 g of TEOS (98%, Aldrich) for unlabeled MCM-41 or 0.46 g of TEOS mixed with 0.02 mL of the spin-label solution in the case of MCM-41 (SL1SiEt). This yields the following molar composition: TEOS; 0.005 SL1SiEt; 0.13 CTAB; 0.6 NaOH; 111 H_2O . The mixture was stirred for 24 h at room temperature after which the solid was separated by filtration and allowed to dry at

ambient temperature for 24 h. This material will be referred to as RT-MCM-41. In the second procedure the molar composition of the reaction gel was as follows: TEOS; 0.002 SL1SiEt; 0.12 CTAB; 2.4 NH₄OH; 74 H₂O. The reaction took place during 4 h at ambient temperature. RT-MCM-41 material was obtained after filtering and washing as described above. Here, also a hydrothermal stage was performed by transferring the reaction mixture to an autoclave at 373 K for 4 days. After cooling to room temperature, the solid material was collected and dried as described above. This material will be referred to as HY-MCM-41. Solvent extraction of HY-MCM-41 was performed by refluxing 1 g of the material for 24 h in 88.5 g of 1.5 wt % HCl/2.5 wt % H₂O/MeOH (Bio Lab Ltd.), according to the procedure of Stein et al.⁴⁵ and the obtained material is termed SE-MCM-41. Calcination was performed by heating the HY-MCM-41 to 873 K in steps of 150 deg per half hour. After 4 h at 873 K, the material was left in the oven to cool for 1 h, subsequently, it was taken out to cool to room temperature. This material will be referred to as CA-MCM-41.

Preparation of the Spin Probe Solutions. Micellar solutions of different spin-labels were prepared using the same molar composition as was used for the MCM-41 synthesis, omitting the base and TEOS. The spin-labels used were 4-hydroxy-TEMPO-benzoate (4HTB), 5-doxylstearic acid (5DSA), and 3-carboxyproxyl (3CP) (all from Aldrich) and SL1SiEt; all are depicted in Figure 1. The concentrations used were 2.25 mM for all the spin-label solutions, except for 4HTB, for which a concentration of 2.25 mM proved to be too high, causing a fast decay in the ESEEM experiments; hence, 1 mM 4HTB solutions were prepared. 4HTB and 5DSA were stored as ethanol solutions, SL1SiEt in its original methanol solution. The solvent was evaporated by a N₂ flow after which the premixed micellar solution was added. The solution of 3CP in D₂O was mixed with deuterated glycerol (Cambridge Isotope Laboratories, Inc.) to produce a glass upon freezing.

Characterization and Spectroscopy. Small-angle X-ray (SAX) diffraction patterns were obtained on a SAX diffractometer, equipped with a Franks mirror and a one-dimensional position sensitive detector (homemade), using Cu K α (1.54 Å) with a Ni-filter.⁴⁶ The surface area and pore size distribution were obtained from nitrogen adsorption–desorption isotherms measured at 77 K with a NOVA-2000 instrument (Quantachrome, version 7.11) using conventional BET and BJH methods. The samples were outgassed under vacuum at 573 K prior to analysis. Chemical analysis was performed at the Microanalysis laboratory of the Hebrew University, Jerusalem.

Solid state ¹³C and ²⁹Si MAS NMR experiments were carried out on a Bruker DSX 300 spectrometer, operating at 75.47 and 59.6 MHz, respectively, with a spinning rate of 5 kHz. ²⁹Si and ¹³C spectra were measured using the Hahn echo sequence with π , $\pi/2$ pulses of 10, 5 μ s, τ of 200 μ s, and the repetition delay was 20 and 5 s, respectively. High power proton decoupling was employed (80 kHz decoupling amplitude) and 1000 and 4000 scans were accumulated for ²⁹Si and ¹³C, respectively. The chemical shift is scaled to ppm from TMS.

All continuous wave (CW) X-band EPR spectra were recorded on a Varian E-12 spectrometer operating at 9 GHz at various temperatures or on a Bruker ER200 D-SRC spectrometer. In all cases a modulation frequency of 100 kHz was applied and the modulation amplitude was 1 G. Three pulse ESEEM experiments (see Figure 2a) were recorded at 50 K on a Bruker Elexsys E 580 spectrometer using four step phase cycling.⁴⁷ The $\pi/2$ pulse length was 16 ns and τ was optimized at each field position (i) to maximize ²H modulation according

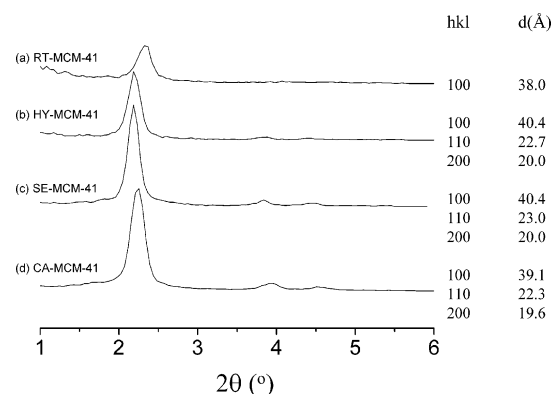


Figure 3. Small-angle X-ray diffraction patterns of (a) RT-MCM-41 (SL1SiEt), (b) HY-MCM-41 (SL1SiEt), (c) SE-MCM-41 (SL1SiEt), and (d) CA-MCM-41.

to $\tau = (2n + 1)/|2\nu_1|$ ($n = 1, 2, \dots$) and (ii) to suppress ¹H modulation according to $\tau = (2n + 1)/|\nu_1|$,⁴¹ where ν_1 is the Larmor frequency of the nucleus to be suppressed or enhanced. The way the empirical modulation depth, $k(^2\text{H})$, was calculated is indicated in Figure 2b. When proton modulation was present, $k(^2\text{H})$ was determined from an average trace (see dotted line in Figure 2b) passing through the proton periods. We have also quantified the modulation depth by a comparison of the intensity of the ²H peak in the Fourier transform of the ESEEM trace and the results obtained were the same. Most ESEEM measurements were recorded at three different field positions. All liquid samples were measured in quartz flat cells, whereas frozen solutions and solid samples for EPR and ESEEM experiments were measured in 3 mm o.d. quartz tubes. The in situ CW EPR measurements were done by transferring a part of the reaction mixture immediately after mixing to the EPR flat cell, and the flat cell remained in the cavity throughout the measurements. The precipitate appeared at the same time in the flat cell and in the reaction vessel. The samples for ESEEM measurements were prepared by quenching small portions of the reaction mixture in liquid nitrogen after different reaction times.

Results

Characterization of the Final Material. SAXS diffraction measurements were performed on all the materials synthesized. Adding the spin probe or using a deuterated surfactant did not have an influence on the degree of ordering. The SAXS diffraction pattern of the room temperature material shows a relatively broad d_{100} peak, consistent with its lower degree of order, as is known from the literature.⁴⁸ The hydrothermal stage, calcination and solvent extraction either improved the structure and/or led to a change in the d -spacing as shown in Figure 3. Upon hydrothermal treatment d increases, it hardly changes after solvent extraction and calcination causes a decrease in the d -spacing, consistent with the literature.^{45,48} Nitrogen adsorption isotherms measured on the calcined and solvent extracted materials gave an average pore size of 28.7 Å (using the BJH method) for both the SE-MCM-41 and the CA-MCM-41. The surface area of both materials, derived from a BET plot, is larger by 2% for the calcined material (926.8 m²/g vs 905.0 m²/g).

The room temperature (~ 298 K) CW EPR spectra of RT-MCM-41 (SL1SiEt), prepared with either NaOH or NH₄OH, and of HY-MCM-41 (SL1SiEt) are the same. The spectrum, shown in Figure 4, is characteristic of the slow motion regime, yet not in the rigid limit.⁴⁹ Its resolved hyperfine features are an indication that no detectable autopolymerization occurred, i.e., that the spin-label is isolated and distributed throughout

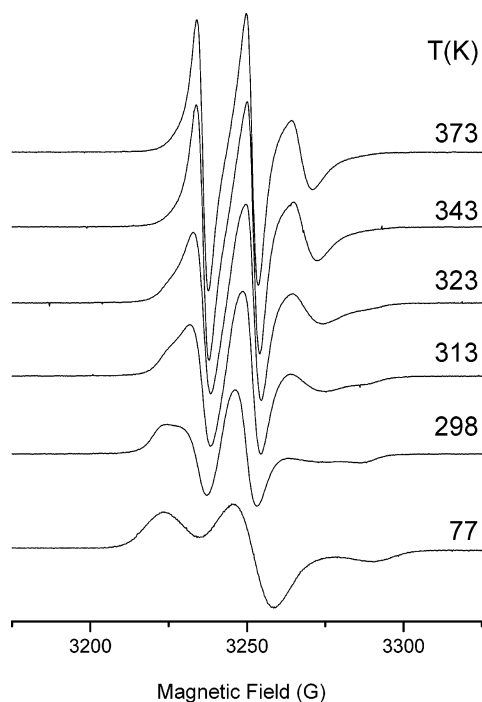


Figure 4. Temperature-dependent CW EPR spectra of RT-MCM-41 (SL1SiEt) recorded at a microwave frequency, ν_{MW} , of 9.19 GHz.

TABLE 1: Results of the Chemical Analysis (C, H, N) of HY-MCM-41 (SL1SiEt) and SE-MCM-41 (SL1SiEt)

	HY-MCM-41 (SL1SiEt)	SE-MCM-41 (SL1SiEt)
% C	26.6	1.8
% H	5.9	1.7
% N	1.6	0.3

the sample. In the case of aggregations, spin exchange would give rise to a broad, single line.⁵⁰ The spectrum recorded at 77 K (bottom trace in Figure 4) exhibits a somewhat broadened powder pattern, which indicates that the average proximity of spin-labels is around 2.5–3.5 nm. This estimate is based on a comparison of the 77 K spectrum with line shapes of a series of homogeneous frozen solutions of 4HTB in toluene. The highest similarity was with spectra in the concentration range of 0.05–0.10 M, which corresponds to average distances between 2.6 and 3.3 nm.⁵¹ The EPR spectra recorded between 313 and 373 K, shown in Figure 4, exhibit reversible changes; as the temperature increases, the spectrum becomes more isotropic, showing the existence of some motional freedom.

Earlier reports in the literature, primarily based on NMR of MCM-41 functionalized during the synthesis,^{28,45} show that extraction removes the template, while the ATEs group remains attached to the silica. Chemical analyses of C, H, and N of the parent HY-MCM-41 (SL1SiEt) and the resulting SE-MCM-41 (SL1SiEt) indeed show that the organic fraction has been almost completely removed after the extraction, as is presented in Table 1. Unfortunately, the extraction procedure, which is carried out in an acidic solution converts the nitroxide radical to diamagnetic hydroxylamine,⁵² eliminating almost completely the EPR signal of SE-MCM-41 (SL1SiEt). Stirring bare SL1SiEt in the solvent extraction mixture (same conditions) revealed that the radical almost totally decomposes after 2 h. ²⁹Si MAS NMR measurements were carried out in an attempt to detect Si–O–C structures in the SE-MCM-41 material but none were observed. This is not surprising considering the low initial amount of SL1SiEt used (TEOS:SL1SiEt = 500) and the fact that only a fraction of it is incorporated in the final material (see below).

It is essential to use such a small amount of spin probe for the observation of a well resolved hyperfine structure and for the application of ESEEM. The ¹³C measurements carried out under cross-polarization conditions did not show any signal. Spectra collected by standard Hahn echo showed a very weak peak at a chemical shift of 50 ppm. This chemical shift is not close to any of the ATEs carbons⁵³ and may arise from carbons of the six-membered ring of the hydroxylamine, which are expected around this chemical shift. The methyl carbons are expected to have lower chemical shifts (around 20 ppm) and it is not clear why they were not observed.

In Situ CW EPR Experiments. In situ CW EPR spectra of the reaction mixture exhibited changes in the line intensity only, and not in the line shape. For example, Figure 5a shows the room-temperature spectrum recorded 9 min and 24 h after the addition of TEOS. A plot of the intensity of the central nitrogen hyperfine line, taken as the difference in intensity between the maximum and the minimum signal amplitude, as a function of time shows that the increase occurs up to 500 min (Figure 5b). The change in intensity indicates that the process taking place is dissolution of the spin probe, due to slow hydrolysis. Initially, SL1SiEt, being hydrophobic, does not dissolve in the aqueous solution and exhibits a broad unresolved line due to spin exchange. A closer look at the 9 min spectrum, depicted in Figure 5a, indeed reveals a broad background, marked with an arrow, on which the sharp triplet is superimposed. This becomes apparent after subtracting the normalized spectrum recorded after 24 h, as shown in the bottom trace of Figure 5a. Once hydrolyzed, the spin probe becomes soluble and isolated, thus exhibiting a well resolved triplet. The same behavior was observed for SL1SiEt added to micelles of CTAB and H₂O, without TEOS nor base. These results are represented in Figure 5b by gray symbols, showing that the hydrolysis of SL1SiEt is slow. From earlier in situ studies, in which surfactant-like spin probes were used to study the formation of MCM-41 under similar conditions, it was clear that the major changes took place in the first 12 min.^{20,21} These were followed by a slow step that lasts about 1 h. Similarly, in situ XRD measurements show that the hexagonal structure is generated within 3 min.¹⁹ This large time scale difference shows that even though the organization of the final hexagonal structure is complete, the hydrolysis of SL1SiEt in the solution continues. The superfluous hydrolyzed SL1SiEt that did not hydrolyze on time to take part in the co-condensation with TEOS, was found in the filtrate, its EPR spectrum being similar to that shown in the middle spectrum of Figure 5a.

The spectrum of the reaction mixture after 24 h consists of a triplet with no indication of any superimposed broader signal, although the sample showed the presence of a white precipitate. Hence, the immobilization of the spin probe in RT-MCM-41 (SL1SiEt), as it is clear from the RT spectrum in Figure 6, only occurs upon drying the material, suggesting that, prior to drying, the silica network is liquidlike (on the EPR time scale). To find out whether this is a reversible process, the following experiment was carried out: RT-MCM-41 (SL1SiEt) was stirred in water for 24 h and the EPR spectrum of the sample, still in water, was recorded (Figure 6A,b). It exhibits a sharp triplet, superimposed on a weak broad signal, marked with an arrow. This indicates that the silica network is far from being fully cross-linked and that the addition of water regenerated the fluidity for some parts of the silica, turning 15% of the silica-bound spin probe into a highly mobile species. This quantification was obtained from a reconstruction of the spectrum by adding the appropriated relative intensities of the RT spectrum of dried

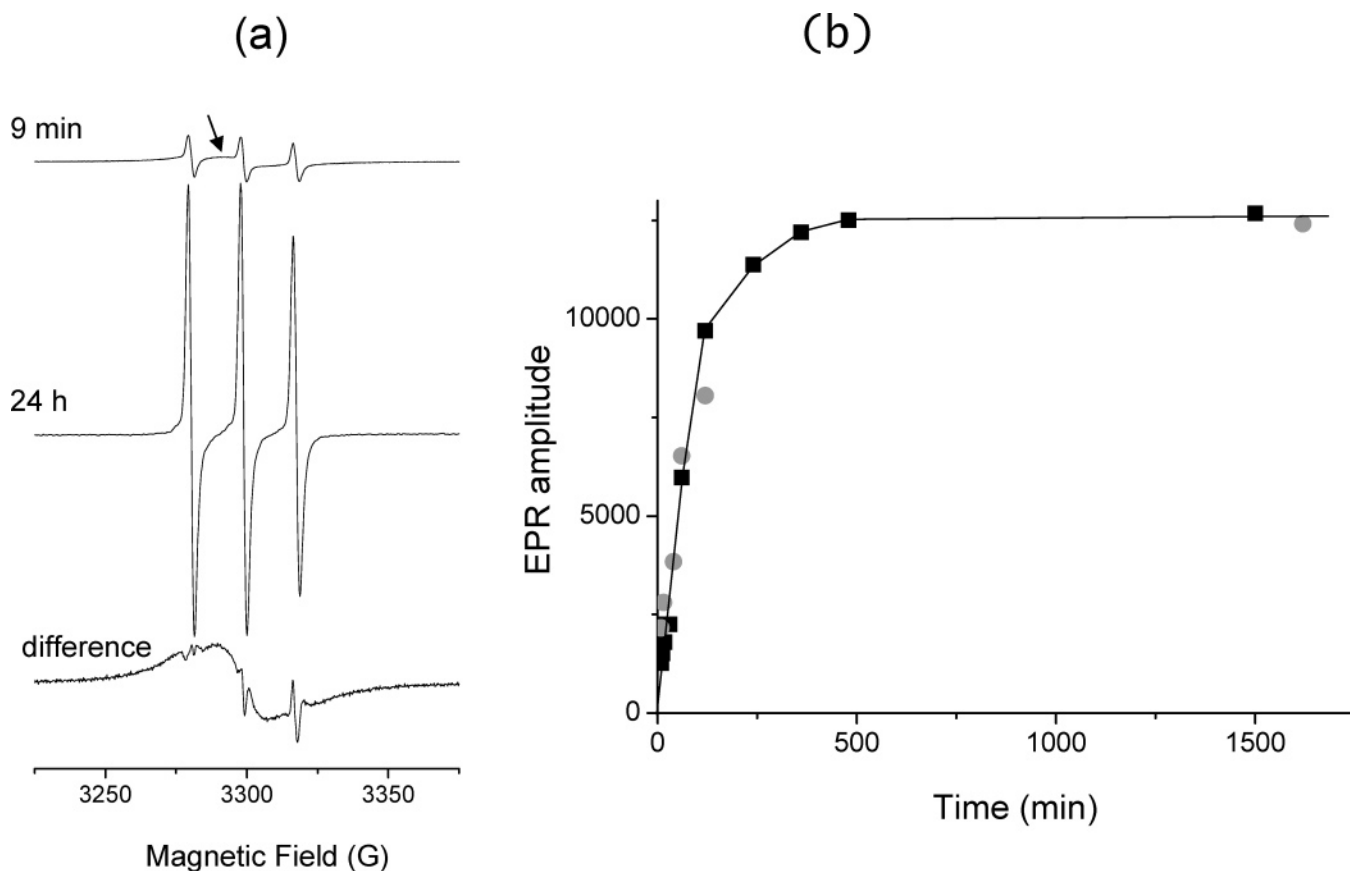


Figure 5. (a) Room-temperature CW EPR spectra of a reaction mixture of MCM-41(SL1SiEt) recorded after 9 min and 24 h ($\nu_{\text{MW}} = 9.78$ GHz) and the difference between the two, after normalization. (b) Intensity of the middle EPR line of the MCM-41(SL1SiEt) reaction mixture (squares) and SL1SiEt in a micellar CTAB solution (circles) as a function of time.

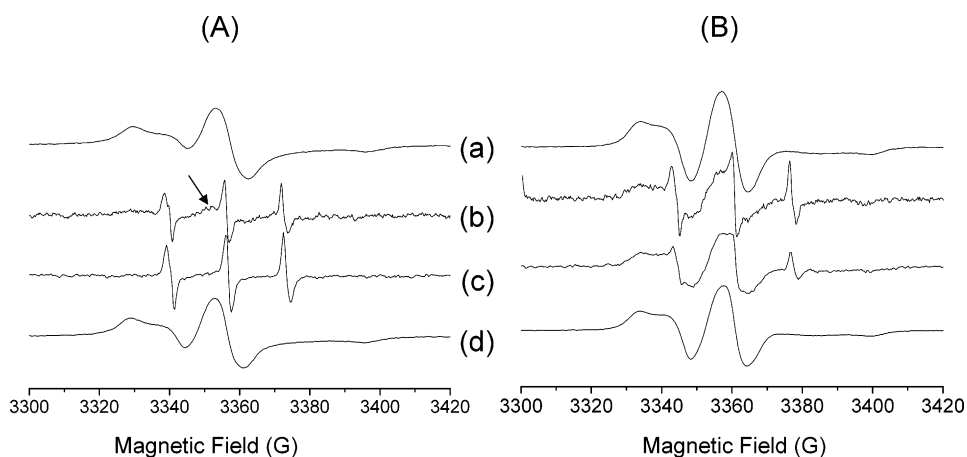


Figure 6. CW EPR spectra of (A) RT-MCM-41 (SL1SiEt) ($\nu_{\text{MW}} = 9.18$ GHz) and (B) HY-MCM-41 (SL1SiEt) ($\nu_{\text{MW}} = 9.52$ GHz). Key: (a) Dry material before stirring, (b) suspension after 24 h stirring in H_2O , (c) suspension after 48 h stirring in H_2O and (d) same as part c after filtering and drying.

RT-MCM-41 (SL1SiEt) (Figure 6A,a) and the sharp triplet (Figure 5a, middle trace). After 48 h in water the relative fraction of the mobile species has increased to $\sim 42\%$ (Figure 6A,c). When the sample was dried again, the original slow motion spectrum was restored, as is evident from Figure 6A,d. The same experiment carried out on HY-MCM-41 (SL1SiEt) showed that only a very small part of the spin-label (3–6%) restored its high mobility upon the addition of water, as shown in Figure 6B. This shows a higher degree of silica cross-linking after the hydrothermal stage and provides further evidence that SL1SiEt has copolymerized with the TEOS. We were not able to measure

the EPR spectrum of the reaction mixture after the hydrothermal stage prior to drying, due to its high viscosity, which prevented the transfer into the EPR flat cell. The increase in the degree of the silica cross-linking upon the hydrothermal stage is also supported by ^{29}Si NMR measurements on samples prepared without SL1SiEt, presented in Figure 7, which shows a significant increase in the $Q^4/(Q^3 + Q^2)$ ratio following the hydrothermal stage. The assignments of the peaks are based on reports in the literature.^{54,55}

ESEEM Experiments. To determine the location of SL1SiEt at any point of the reaction, ESEEM measurements were carried

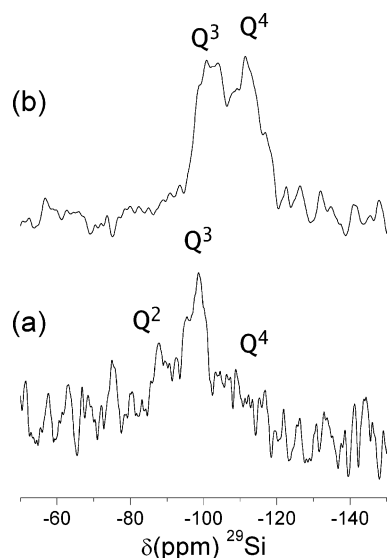


Figure 7. ^{29}Si MAS NMR spectra of (a) RT-MCM-41 and (b) HY-MCM-41 (prepared with NH_4OH).

out, first on reference solutions, then on reaction mixtures quenched after different reaction times and in the final materials. A typical three pulse ESEEM waveform, in this case of RT-MCM (SL1SiEt) prepared with CTAB- d_9 , is depicted in Figure 2b. ESEEM experiments have to be carried out at low temperatures (50 K) to slow the echo decay and to eliminate averaging of the hyperfine anisotropy by motion. Therefore, the experiments were carried out on reaction mixtures that were quenched by rapid freezing in liquid nitrogen. It has already been shown that upon such a rapid freezing the micellar structure is preserved.^{22,25,56}

Micellar Solutions. CTAB micellar solutions containing spin-labels with known locations in the micelle, based on their hydrophilicity and previous studies^{21,22,24} were used as references for the determination of the location of SL1SiEt within the micelle. The hydrophobic 4HTB is expected to be found in the hydrophobic core, whereas the hydrophilic 3CP is located in the hydrophilic outer region of the micelle, or in the water solution. The amphiphilic 5DSA, on the other hand, will be oriented along the surfactant molecules with its negatively charged headgroup near the CTAB headgroup and the nitroxide label located somewhat further down into the core of the micelle. The structures of these spin probes are shown in Figure 1. Two specifically deuterated surfactants, CTAB- d_2 , deuterated in the α position, and CTAB- d_9 with a perdeuterated ammonium headgroup, were used to determine the location of these spin probes with respect to the micellar interface. In addition, a solution containing regular CTAB in D_2O and a solution containing only D_2O without surfactant, were also used as reference systems. The results of the comparative three pulse ESEEM measurements of the micellar solutions are presented in Figure 8. Measurements were carried out at different field positions and on different samples to verify the reproducibility. Since the modulation depth is field dependent, comparison can be carried out only between measurements performed at the same magnetic field and τ value. For the sake of clarity, only the results from the field at which the echo is maximum are shown for each spin probe. The same trends were observed for all fields measured. In those cases where the measurements were performed more than once, an error bar indicates the spread of the results.

The $k(^2\text{H})$ values in the CTAB- d_2 /H $_2$ O system, shown in Figure 8a, are rather small, nonetheless, they show that 5DSA

exhibits the largest $k(^2\text{H})$ value and that it is slightly higher than that of SL1SiEt. In contrast, the $k(^2\text{H})$ values in the CTAB- d_9 /H $_2$ O systems are significantly higher (Figure 8b), due to the larger number of deuterons. It is apparent that the $k(^2\text{H})$ of the three reference probes decreases in the order: 3CP > 5DSA > 4HTB, in agreement with their increasing hydrophobicity. In this series the $k(^2\text{H})$ of SL1SiEt is close to that of 3CP. The modulation depths obtained in the CTAB/D $_2$ O system (Figure 8c) show that the 3CP probe experiences the strongest ^2H modulation, whereas the $k(^2\text{H})$ for the two other spin probes is about the same. The difference in $k(^2\text{H})$ of 3CP in the micelles of CTAB/D $_2$ O vs that obtained in D $_2$ O without surfactant (Figure 8d) shows that the 3CP is indeed located close to the micelle–water interface and not in the surrounding solution. When comparing $k(^2\text{H})$ of hydrolyzed SL1SiEt in all the systems, it becomes clear that this spin-label must be situated somewhere between 3CP and 5DSA when it is dissolved in a micellar CTAB/H $_2$ O solution. The relative location of all the investigated spin probes is schematically shown in Figure 8e. In all the experiments above, the non-hydrolyzed SL1SiEt does not contribute to the echo due to its fast relaxation rate, as indicated by the absence of a broad singlet in the echo-detected EPR spectrum (not shown).

Final Products and Reaction Mixtures. While considering the $k(^2\text{H})$ values of SL1SiEt in the reaction mixture, one has to take into account the fact that some of the SL1SiEt hydrolyzed after the formation of the MCM-41 structure, as evidenced by the in situ EPR experiments. The echo intensity was found to increase as the reaction progresses due to the slow hydrolysis, consistent with the CW EPR results. Therefore, the $k(^2\text{H})$ will have contributions from the spin probes incorporated into the silica layer and from those that remain in the solution. To discern the contributions of the two, we have recorded the ESEEM trace of the filtrate of a reaction mixture of RT-MCM-41 (SL1SiEt) with CTAB- d_9 /H $_2$ O after 24 h and no ^2H modulation was observed. Consequently, the presence of a nonincorporated SL1SiEt in the mixture leads to a net reduction in $k(^2\text{H})$ when CTAB- d_9 is used, since the dissolved spin probe also contributes to the echo. This has a more pronounced effect at times longer than 1 h, after which the structure has formed.²⁰ Indeed, a reduction in the modulation depth was observed when comparing samples quenched after 8 min, 2 h, and 24 h ($k(^2\text{H}) = 0.09, 0.04, 0.03$, respectively), which may be a consequence of nonincorporated SL1SiEt at long times. In Figure 9, a considerable reduction in $k(^2\text{H})$ is noted for the samples prepared with CTAB- d_9 , from 0.48 in the micellar solution to 0.09, 8 min after the addition of TEOS. This indicates that the spin-labels move further away from the polar headgroup region, once they become part of the silica oligomers. Then, an increase in $k(^2\text{H})$ is observed for RT-MCM-41 (SL1SiEt) prepared with CTAB- d_9 (Figure 9). For samples prepared with NH_4OH instead of NaOH, we obtain a comparable modulation depth for the RT-MCM (SL1SiEt). In this case it was also shown that hydrothermal treatment, in contrast to drying, does not change the position of the spin-label with respect to the polar head region (results not shown). Interestingly, the $k(^2\text{H})$ of 5DSA in the micelles, the reaction mixture and RT-MCM-41 (SL1SiEt) prepared with CTAB- d_9 exhibited only subtle variations as shown in Figure 9.

When ESEEM measurements are performed on reaction mixtures containing SL1SiEt in systems with CTAB- d_2 or D $_2$ O quenched at different reaction times, it becomes apparent that $k(^2\text{H})$ does not change significantly throughout the reaction. A comparison between the $k(^2\text{H})$ values in the micelles, the

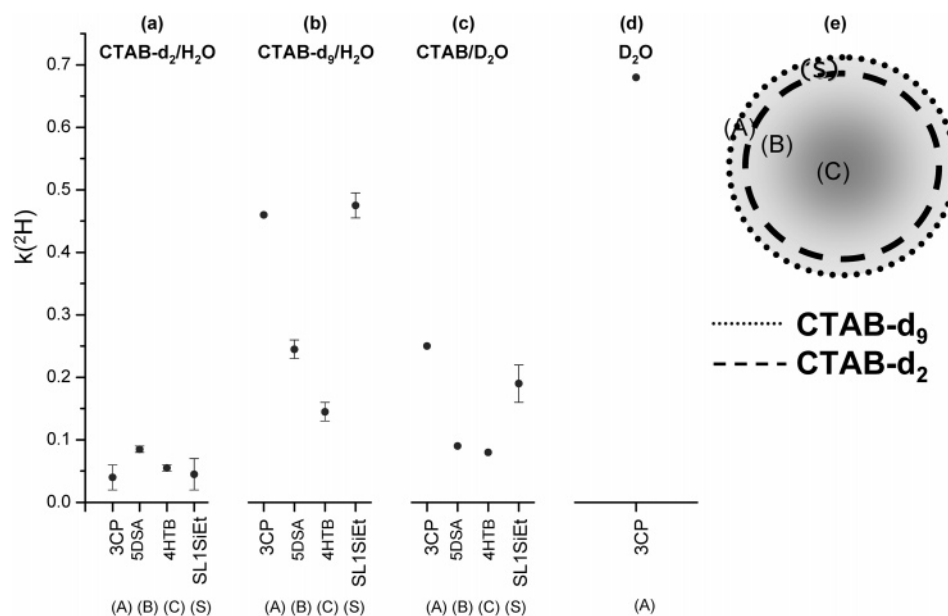


Figure 8. $k(^2\text{H})$ of 3CP (A), 5DSA (B), 4HTB (C), and SL1SiEt (S) in solutions of (a) CTAB- d_2 /H $_2$ O, (b) CTAB- d_9 /H $_2$ O, (c) CTAB/D $_2$ O, and (d) D $_2$ O without surfactant. (e) Schematic representation of the location of the spin probes within the micelles of CTAB. The dotted and dashed lines represent the perimeters of the deuterons in CTAB- d_9 and CTAB- d_2 , respectively.

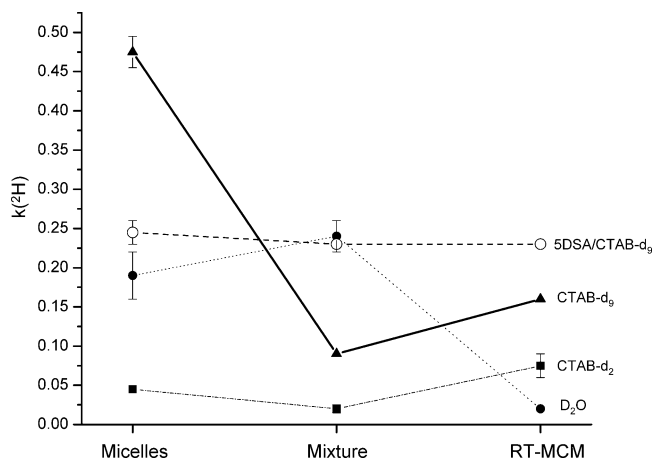


Figure 9. Comparison of the $k(^2\text{H})$ of SL1SiEt in a CTAB micellar solution (denoted as Micelles), a reaction mixture of MCM-41 (denoted as Mixture) and RT-MCM-41 (SL1SiEt) (denoted as RT-MCM) prepared with CTAB- d_2 /H $_2$ O, CTAB- d_9 /H $_2$ O and CTAB/D $_2$ O (denoted as D $_2$ O). The empty circles are the results of the corresponding 5DSA samples for comparison.

reaction mixture and in RT-MCM-41 (SL1SiEt) is shown in Figure 9. The behavior of the CTAB- d_2 system is similar to that of CTAB- d_9 , only the modulation depth is significantly shallower and therefore the absolute difference is smaller. As for the D $_2$ O system, the most significant change occurs upon filtering and drying to obtain RT-MCM-41 (SL1SiEt), which shows almost no modulation, as was expected.

Discussion

Monitoring the incorporation of a siloxane-based spin probe that copolymerizes with the silica source provides new insights into the properties of MCM-41 during its various formation stages. While earlier EPR studies concentrated on the properties of the organic phase, this work provides information regarding the silica layer. The observation of a relatively large $k(^2\text{H})$ for CTAB- d_9 and a significant $k(^2\text{H})$ for CTAB- d_2 , which are between the values of 3CP and 5DSA shows that, once hydrolyzed and in the absence of TEOS, SL1SiEt is situated in

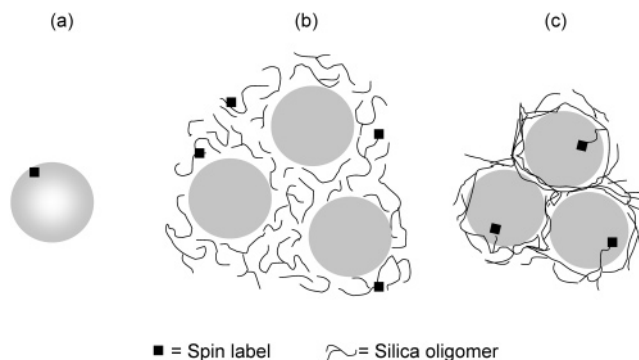


Figure 10. Schematic representation of the different stages of the reaction (a) after initial hydrolysis of the spin-label in the micellar solution (the gray circle represents the micelle), (b) after the addition of TEOS and base, and (c) after drying the material. In parts b and c, the gray circles represent a cross section of the organic aggregate. Only part of the hexagonal structure is drawn, due to space considerations.

the micelle–water interface region. From this we conclude that the hydrolyzed silicate is at the interface, interacting with the positive headgroups of the surfactants. The slow polymerization rate of the hydrolyzed SL1SiEt and its very low concentration allowed the isolation and observation of this interaction. This finding, therefore, provides experimental evidence for the principle of charge matching at the interface and the cooperative self-assembly mechanism formulated by Chmelka, Stucky, and co-workers.^{12,15} There, a preferential adsorption of the silicate at the micellar interface was postulated as the first step of the formation mechanism. This is in contrast to the suggested mechanism of Zana and co-workers where the silicate oligomers do not adsorb on the micelle interface but instead form siliceous prepolymers that bind free surfactants.¹¹

When SL1SiEt is added together with TEOS, under conditions where hydrolysis and polymerization occur simultaneously, the copolymerization with TEOS pushes the spin-label away from the micellar interface region, into a silica network forming around the micelle, as shown in Figure 10. This layer is highly fluid, since the spin probe exhibits a fast limit isotropic spectrum. The high degree of fluidity of the silica network during the room temperature stage of the reaction, prior to drying, is unexpected,

especially in light of the earlier in situ EPR studies carried out with surfactant-like spin probes under the same conditions.^{20,21} There, spectra typical of slow motion were observed, moreover, a clear, gradual decrease in the spin-label's mobility was detected as the reaction progressed. Two distinct stages were observed in the time evolution of the reaction, of which the first, lasting about 12 min was attributed to the formation of silica oligomers and the hexagonal structure and a second, longer period (~ 1 h) with less pronounced changes was said to be caused by a further polymerization of the silica network. These stages were not detected here, due to the fast limit character of the spectrum of SL1SiEt throughout the reaction. Thus, indicating that, while the surfactant molecules within the organic aggregates are closely packed and experience increased ordering, the forming silica layer around the aggregates is locally highly disordered and liquidlike. This observation is also consistent with the absence of a ^2H quadrupolar coupling of D_2O in the silicate-liquid crystal phase reported by Chmelka and co-workers.^{14,15} In this case the majority of the water signal should originate from the silicate layer and not from water situated in the micellar polar headgroup region. A high fluidity of the silica layer was also reported for SBA-15 prior to drying.²⁴ There, this was deduced from Pluronics that were spin-labeled at the end of their PEO chains, which were found to penetrate into the silica layer. Their isotropic fast (on the EPR time scale) limit spectrum indicated that the silica layer is fluid enough to allow fast, isotropic motion. In situ XRD studies of the formation of MCM-41 with TEOS as a silica source showed that the hexagonal order is formed within 3 min,¹⁹ consistent with the increased ordering within the organic aggregates upon the organization of the hexagonal structure. Our results show that prior to drying or hydrothermal treatment, the organic assemblies are spaced by a loosely linked, highly fluid silica layer (see Figure 10).

The filtration/drying process leads to the removal of the water in the silicate layer and to its contraction, as illustrated in Figure 10 and in agreement with the decrease in the d_{100} spacing observed by Lindén et al.¹⁹ This is accompanied by a considerable reduction in the motion of the silica-attached spin-label and an increase in $k(^2\text{H})$ of the CTAB- d_9 and CTAB- d_2 . This indicates that in the dry solid material, the pending spin-probe chain protrudes into the organic phase. Comparison of the $k(^2\text{H})$ values with those of the reference spin probes in the CTAB micellar solution places the nitroxide of SL1SiEt in the final material deeper into the organic region, lower than position 5 on the carbon chain. In the RT material, the cross-linking degree of the silica is rather low and its mobility can therefore readily be restored by the addition of water. In the materials prepared with the hydrothermal stage, the silica layer is significantly better cross-linked and the fluidity observed, prior to the hydrothermal stage, cannot be restored upon the addition of water. The low degree of the cross-linking of the silica during the room temperature formation therefore allows for phase transitions upon change of pH, temperature, or any other parameter that affects the organization of the composite silica-organic mesophase.^{57,58} Figure 10 summarizes the three steps of the formation mechanism evident from this work and earlier in-situ XRD reports.¹⁹

The formation of the silica layer during the synthesis of MCM-41 has also been the focus of an in-situ IR study. In this study the time evolution of Si–O vibrations associated with Q^3 and Q^4 sites was followed.¹⁷ The silica source was fumed silica and it took 24 h for the hexagonal structure to appear. The growth rate of Q^3 at different temperatures was then used

to determine the activation energy. Under these reaction conditions, the rate-determining step was found to be the base assisted hydrolysis of the silica source and not the generation of the hexagonal structure. This is in contrast to our reaction conditions where the TEOS hydrolysis is very fast.

Conclusions

In situ CW EPR and ESEEM of a siloxane derived spin probe, SL1SiEt, allowed to explore the properties of the silica layer during the formation of MCM-41. Experimental evidence for the location of the hydrolyzed spin probe in close vicinity to the surfactants' polar heads was obtained for low concentrations of the spin probe in CTAB micellar solutions. This supports the postulation of charge matching at the interface as a driving force for the formation of the mesostructure, introduced by Stucky and co-workers.¹⁴ Once TEOS and base are added silicate polymerization takes place and a highly fluid silica layer is formed around the micelles. This layer remains fluidlike in room temperature reactions as long as no filtering and drying takes place. Removal of the water significantly hardens the silica layer, considerably restricting the motion of the silica-bound spin probe. Reintroduction of water to dried MCM-41 formed at room temperature restores the fluidity, indicating a low degree of cross-linking. In contrast, the fluidity cannot be restored in MCM-41 prepared with an additional hydrothermal stage, due to a significantly higher level of silica cross-linking.

Acknowledgment. This research was supported by the center of excellence Origin of Ordering and Functionality in Mesos-structured Hybrid Materials supported by The Israel Science Foundation (Grant No. 800301-1). The Gerhard M. J. Schmidt Minerva Center for Supramolecular Architecture (Minerva is funded through the BMBF) and the Ilse Katz Institute for Material Science and Magnetic Resonance Research are acknowledged for their kind support.

References and Notes

- (1) Kresge, C. T.; Leonowicz, M. E.; Roth, W. J.; Vartuli, J. C.; Beck, J. S. *Nature* **1992**, *359*, 710–712.
- (2) Beck, J. S.; Vartuli, J. C.; Roth, W. J.; Leonowicz, M. E.; Kresge, C. T.; Schmitt, K. D.; Chu, C. T.-W.; Olson, D. H.; Sheppard, E. W.; McCullen, S. B.; Higgins, J. B.; Schlenker, J. L. *J. Am. Chem. Soc.* **1992**, *114*, 10834–10843.
- (3) Zhao, X. S.; Lu, G. Q.; Millar, G. J. *Ind. Eng. Chem. Res.* **1996**, *35*, 2075–2090.
- (4) Selvam, P.; Bhatia, S. K.; Sonwane, C. G. *Ind. Eng. Chem. Res.* **2001**, *40*, 3237–3261.
- (5) Davis, M. E. *Nature (London)* **2002**, *417*, 813–821.
- (6) Ying, J. Y.; Mehnert, C. P.; Wong, M. S. *Angew. Chem., Int. Ed. Engl.* **1999**, *38*, 56–77.
- (7) Myers, D. *Surfactant Science and Technology*; VCH: New York, 1992.
- (8) Patarin, J.; Lebeau, B.; Zana, R. *Curr. Opin. Colloid Interface Sci.* **2002**, *7*, 107–115.
- (9) Attard, G. S.; Glyde, J. C.; Goeltner, C. G. *Nature (London)* **1995**, *378*, 366–368.
- (10) Huo, Q.; Margolese, D. I.; Ciesla, U.; Demuth, D. G.; Feng, P.; Gier, T. E.; Sieger, P.; Firouzi, A.; Chmelka, B. F.; Schüth, F.; Stucky, G. D. *Chem. Mater.* **1994**, *6*, 1176–1191.
- (11) Frasch, J.; Lebeau, B.; Soulard, M.; Patarin, J. *Langmuir* **2000**, *16*, 9049–9057.
- (12) Monnier, A.; Schüth, F.; Huo, Q.; Kumar, D.; Margolese, D.; Maxwell, R. S.; Stucky, G. D.; Krishnamurty, M.; Petroff, P.; Firouzi, A.; Janicke, M.; Chmelka, B. F. *Science* **1993**, *261*, 1299–1303.
- (13) Huo, Q.; Margolese, D. I.; Ciesla, U.; Feng, P.; Gier, T. E.; Sieger, P.; Leon, R.; Petroff, P. M.; Schüth, F.; Stucky, G. D. *Nature* **1994**, *368*, 317–320.
- (14) Firouzi, A.; Atef, F.; Oertli, A. G.; Stucky, G. D.; Chmelka, B. F. *J. Am. Chem. Soc.* **1997**, *119*, 3596–3610.
- (15) Firouzi, A.; Kumar, D.; Bull, L. M.; Besier, T.; Sieger, P.; Huo, Q.; Walker, S. A.; Zasadzinski, J. A.; Glinka, C.; Nicol, J.; Margolese, D.; Stucky, G. D.; Chmelka, B. F. *Science* **1995**, *267*, 1138–1143.

- (16) Chen, C.-Y.; Burkett, S. L.; Li, H.-X.; Davis, M. E. *Microporous Mater.* **1993**, 2, 27–34.
- (17) Holmes, S. M.; Zholobenko, V. L.; Thursfield, A.; Plaisted, R. J.; Cundy, C. S.; Dwyer, J. J. *Chem. Soc., Faraday Trans.* **1998**, 94, 2025–2032.
- (18) Ortlam, A.; Rathouský, J.; Schulz-Ekloff, G.; Zukal, A. *Microporous Mater.* **1996**, 6, 171–180.
- (19) Lindén, M.; Schunk, S. A.; Schüth, F. *Angew. Chem., Int. Ed. Engl.* **1998**, 37, 821–823.
- (20) Zhang, J.; Luz, Z.; Goldfarb, D. *J. Phys. Chem. B* **1997**, 101, 7087.
- (21) Zhang, J.; Luz, Z.; Zimmermann, H.; Goldfarb, D. *J. Phys. Chem. B* **2000**, 104, 279–285.
- (22) Zhang, J.; Carl, P. J.; Zimmermann, H.; Goldfarb, D. *J. Phys. Chem. B* **2002**, 106, 5382–5389.
- (23) Galarneau, A.; Renzo, F.; Fajula, F.; Mollo, L.; Fubini, B.; Ottaviani, M. F. *J. Colloid Interface Sci.* **1998**, 201, 105.
- (24) Ruthstein, S.; Frydman, V.; Kababya, S.; Landau, M.; Goldfarb, D. *J. Phys. Chem. B* **2003**, 127, 1739–1748.
- (25) Ruthstein, S.; Frydman, V.; Goldfarb, D. *J. Phys. Chem. B* **2004**, 108, 9016–9022.
- (26) Shames, A.; Lev, O.; Iosefzon-Kuyavskaya, B. *J. Non-Cryst. Solids* **1994**, 175, 14–20.
- (27) Asefa, T.; Kruk, M.; MacLachlan, M. J.; Coombs, N.; Grondy, H.; Jaroniec, M.; Ozin, G. A. *J. Am. Chem. Soc.* **2001**, 123, 8520–8530.
- (28) Fowler, C. E.; Burkett, S. L.; Mann, S. *Chem. Commun.* **1997**, 1769–1770.
- (29) Melde, B. J.; Holland, B. T.; Blanford, C. F.; Stein, A. *Chem. Mater.* **1999**, 11, 3302–3308.
- (30) Shea, K. J.; Loy, D. A. *Chem. Mater.* **2001**, 3306–3319.
- (31) Oviatt, H. W.; Shea, K. J.; Small, J. H. *Chem. Mater.* **1993**, 5, 943–950.
- (32) Macquarrie, D. J.; Jackson, D. B.; Mdoe, J. E. G.; Clark, J. H. *New J. Chem.* **1999**, 23, 539–544.
- (33) Vansant, E. F.; Van der Voort, P.; Vrancken, K. C. *Characterization and chemical modification of the Silica Surface*; Elsevier: Amsterdam, 1995; p 176.
- (34) Stein, A.; Melde, B. J.; Schroden, R. C. *Adv. Mater.* **2000**, 12, 1403 and references therein.
- (35) Wight, A. P.; Davis, M. E. *Chem. Rev.* **2002**, 102, 3589 and references therein.
- (36) Mann, S.; Burkett, S. L.; Davis, S. A.; Fowler, C. E.; Mendelson, N. H.; Sims, S. D.; Walsh, D.; Whilton, N. *Chem. Mater.* **1997**, 9, 2300 and references therein.
- (37) Ciriminna, R.; Blum, J.; Avnir, D.; Pagliaro, M. *Chem. Commun.* **2000**, 1441 and references therein.
- (38) Caldararu, H.; Caragheorgheopol, A.; Savonea, F.; Macquarrie, D. J.; Gilbert, B. C. *J. Phys. Chem. B* **2003**, 107, 6032–6038.
- (39) Kolling, O. W. *Anal. Chem.* **1977**, 49, 591–594.
- (40) Kevan, L. In *Modern Pulsed and Continuous-Wave Electron Spin Resonance*; Kevan, L., Bowman, M. K., Eds.; Wiley: New York, 1990.
- (41) Kevan, L. In *Time Domain Electron Spin Resonance*; Kevan, L., Schwartz, R. N., Eds.; John Wiley & Sons: New York, 1979.
- (42) Macdonald, P. M.; Rydall, J.; Kuebler, S. C.; Winnik, F. M. *Langmuir* **1991**, 7, 2602.
- (43) Semchyschyn, D. J.; Carbone, M. A.; Macdonald, P. M. *Langmuir* **1996**, 12, 253.
- (44) Zimmermann, H. *Liquid Cryst.* **1989**, 4, 591–618.
- (45) Lim, M. H.; Blanford, C. F.; Stein, A. *J. Am. Chem. Soc.* **1997**, 119, 4090.
- (46) Cheetham, J. J.; Wachtel, E.; Bach, D.; Epand, R. M. *Biochemistry* **1989**, 28, 8928.
- (47) Fauth, J. M.; Schweiger, A.; Braunschweiler, L.; Forrer, J.; Ernst, R. R. *J. Magn. Reson.* **1986**, 66, 74.
- (48) Edler, K. J.; White, J. W. *J. Chem. Soc., Chem. Commun.* **1995**, 155–156.
- (49) Schneider, D. J.; Freed, J. H. In *Biological Magnetic Resonance. Spin Labeling*; Berliner, L. J., Reuben, J., Eds.; Plenum: New York, 1989; Vol. 8; Chapter 1.
- (50) Wertz, J. E.; Bolton, J. R. *Electron Spin Resonance: Elementary Theory and Practical Applications*; McGraw-Hill: New York, 1972; pp 201–203.
- (51) Ruthstein, S.; Artzi, R.; Goldfarb, D.; Naaman, R. *Phys. Chem. Chem. Phys.* **2005**, 7, 524–529.
- (52) Rozantsev, E. G. *Free Nitroxyl Radicals*; Plenum Press: New York, 1970.
- (53) Sadasivan, S.; Khushalani, D.; Mann, S. *J. Mater. Chem.* **2003**, 13, 1023–1029.
- (54) Maciel, G. E.; Sindorf, D. W.; Bartuska, V. J. *J. Chromatogr.* **1981**, 205, 438–443.
- (55) Sindorf, D. W.; Maciel, G. E. *J. Am. Chem. Soc.* **1981**, 103, 4263–4265.
- (56) Ottaviani, M. F.; Daddi, R.; Brustolon, M.; Turro, N. J.; Tomalia, D. A. *Langmuir* **1999**, 15, 1973–1980.
- (57) Matijasic, A.; Voegtlin, A.-C.; Patarin, J.; Guth, J. L.; Huve, L. *Chem. Commun.* **1996**, 1123–1124.
- (58) Landry, C. C.; Tolbert, S. H.; Gallis, K. W.; Monnier, A.; Stucky, G. D.; Norby, P.; Hanson, J. C. *Chem. Mater.* **2001**, 13, 1600–1608.